

Transverse electron momentum distribution in tunneling and over the barrier ionization by laser pulses with varying ellipticity

I. A. Ivanov^{1,2,*}, A.S.Kheifets², J.E. Calvert³, S. Goodall³, X. Wang³,
Han Xu³, A.J. Palmer³, D. Kielpinski³, I.V. Litvinyuk³, and R.T.Sang³

¹*Center for Relativistic Laser Science, Institute for Basic Science, Gwangju 500-712, Republic of Korea*

²*Research School of Physics and Engineering, The Australian National University, Canberra ACT 0200, Australia and*

³*School of Natural Sciences and Centre for Quantum Dynamics, Griffith University, Brisbane QLD 4111, Australia*

(Dated: April 20, 2019)

We study transverse electron momentum distribution (TEMED) in strong field atomic ionization driven by laser pulses with varying ellipticity. We show, both experimentally and theoretically, that the TEMD in the tunneling and over the barrier ionization regimes evolves in a qualitatively different way when the ellipticity parameter describing polarization state of the driving laser pulse increases.

PACS numbers: 32.80.Rm 32.80.Fb 42.50.Hz

A highly non-linear interaction of ultra-short light pulses with matter enabled the measurement of electron dynamics on the atomic time scale and facilitated emergence of the attosecond science [1]. The electric field of the pulse near its peak can be so strong that it becomes comparable to the electric field that binds an electron to an atom or a molecule. The combination of such a light pulse and the Coulomb potential creates a potential barrier which can be tunneled through by the electron and be subsequently ionized. This is a fundamental photoionization event which gives rise to processes such as above-threshold ionization, high harmonic generation, and rescattering phenomena leading to non-sequential double ionization [1]. There are three photoionization regimes in strong-field photoionization; multiphoton ionization (MPI), tunnel ionization and over-the-barrier ionization (OBI). MPI is in the perturbative regime of strong-field interactions in which multiple photons are absorbed in order to photoionize an electron from matter. Tunnel ionization and OBI are ionization events due to the suppression of the Coulomb barrier with OBI being the complete suppression of the barrier. At present no experimental method exists that can distinguish the boundary between tunnel ionization and OBI.

The current understanding of strong field atomic ionization is based on the pioneering work by Keldysh [2] which introduced the well-known distinction between the multiphoton and tunneling ionization regimes. The borderline between the two regimes is drawn by the Keldysh parameter $\gamma = \omega\sqrt{2I}/E$ defined via the frequency ω and the strength E of the laser field and the ionization potential I of the target atom (the atomic units are used in the paper unless otherwise specified). The values of $\gamma \ll 1$ correspond to the tunneling regime. A finer distinction arises when one realizes that the Keldysh theory in its original form is not applicable for very high field strengths exceeding the over the OBI limit. The OBI regime was first observed in [3] (see also [4] for a detailed review). The reason for failure of the Keldysh theory in its original form in the OBI regime is that for the fields exceeding E_{obi} there is a classical escape trajectory for an electron. One can-

not, therefore, rely on the saddle point method that Keldysh employed in his original work. The so-called Keldysh-Faisal-Reiss (KFR) theory [5, 6] must be used instead to describe the OBI regime. Despite the fact that underlying physics is very different in the two regimes (a classically forbidden trajectory for tunneling and a classically allowed trajectory for OBI), the energy spectra and electron angular distributions as given by these two theories are not dissimilar. This makes it often difficult to distinguish the two regimes in the experiment [4].

In this Letter, we demonstrate, that the transverse electron momentum (TEMED) distribution is a measurable quantity that is qualitatively different in the tunneling and the OBI regimes. This distribution gives the probability to detect a photoelectron with a given value of the momentum component p_{\perp} perpendicular to the polarization plane of the laser radiation. In the tunneling regime, TEMD exhibits a cusp-like structure due to the Coulomb focusing effect at $p_{\perp} = 0$ for linear polarization [7], and a Gaussian-like structure predicted by the Keldysh theory for circular polarization [8]. We studied this transition from the cusp-like to the Gaussian structures in detail in the tunneling regime [9], and interpreted this transition as a gradual diminishing of the role of the Coulomb effects with a growing ellipticity of the laser pulse. Further study of the role of the Coulomb focusing effects has been reported in [10]. We shall see below that the situation is quite different in the OBI regime, where the TEMD always has a cusp regardless of the value of the ellipticity parameter. As a result of this qualitatively different behavior of the TEMD, one can clearly distinguish the tunneling and OBI regimes. This is a very important result since the TEMD conveys information about the fine details of the strong field ionization process [11, 12]. One such detail is the electron velocity distributions at the moment of time when ionization occurs, the fact which is often used in various models of strong field ionization. Qualitative difference in TEMD that we demonstrate in the present work implies equally profound difference in the details of the ionization process in the tunneling and OBE regimes.

In the present experiment, we measure TEMD in two atomic species with markedly different ionization potentials. We use the argon atom in the ground 1S_0 state and the neon atom in the 3P_2 metastable state with the ionization potentials of 15.76 eV and 5.07 eV, respectively. This difference in the

*Electronic address: Igor.Ivanov@anu.edu.au

ionization potentials enables the use of the same laser system to access the tunneling and OBI regimes. This measurement using metastable neon is the first time this atomic species was used in a strong-field ionization experiment.

Our theoretical results are obtained by solving the time-dependent Schrödinger equation (TDSE). To describe the field-free Ar and metastable Ne^* atoms, we used effective one-electron potentials [13]. Interaction of the atom with the laser pulse is described in the velocity form of the interaction operator. The laser pulse is elliptically polarized and propagates along the z -direction assumed to be the quantization axis:

$$E_x = \frac{E}{\sqrt{1+\varepsilon^2}} f(t) \cos \omega t, \quad E_y = \frac{E\varepsilon}{\sqrt{1+\varepsilon^2}} f(t) \sin \omega t, \quad (1)$$

where ε is the ellipticity parameter. The function $f(t) = \sin^2(\pi t/T_1)$, with T_1 being the total pulse duration, is used to represent the pulse envelope. For the Ar atom, the field strength was $E = 0.1171$ a.u. corresponding to the peak intensity of 4.8×10^{14} W/cm². For the metastable Ne^* atom, $E = 0.0756$ a.u. with the peak intensity of 2×10^{14} W/cm². The carrier wavelength $\lambda = 750$ nm and the FWHM of 6.5 fs were the same for Ar and Ne^* .

To solve the TDSE we employ the strategy used in the previous works [9, 14, 15]. The solution of the TDSE is represented as a partial waves series:

$$\Psi(\mathbf{r}, t) = \sum_{l=0}^{L_{\max}} \sum_{\mu=-l}^l f_{l\mu}(r, t) Y_{l\mu}(\theta, \phi). \quad (2)$$

The radial part of the TDSE is discretized on the grid with the stepsize $\delta r = 0.1$ a.u. in a box of the size $R_{\max} = 400$ a.u. The maximum orbital momentum in Eq. (2) was restricted to $L_{\max} = 60$. A series of routine checks was performed to ensure the convergence with respect to variation of δr , R_{\max} and L_{\max} . The matrix iteration method [16] was used to propagate TDSE in time.

Ionization amplitudes $a(\mathbf{p})$ were obtained by projecting the solution of the TDSE after the end of the pulse on the set of the ingoing scattering states $\Psi_{\mathbf{p}}^-(\mathbf{r})$ of the target atom. The TEMD $W(p_{\perp})$ was calculated as

$$W(p_{\perp}) = \int |a(\mathbf{p})|^2 dp_x dp_y, \quad p_{\perp} \equiv p_z \quad (3)$$

This is to be compared with the Keldysh theory expression valid in the tunneling regime [17]:

$$W(p_{\perp}) \propto \exp \left\{ -(2I)^{1/2} E^{-1} \sqrt{1+\varepsilon^2} p_{\perp}^2 \right\}. \quad (4)$$

A schematic representation of the experiment is shown in Figure 1. The ultrafast light pulses are produced by a commercially available chirped-pulse amplification laser system (Femtolasers, Femtopower Compact Pro CE Phase). The light pulses are generated, stretched, amplified and then compressed in the system. The pulse repetition rate is 1kHz with a pulse duration of 6 fs, pulse energies of approximately 450 μJ and a central wavelength of 800 nm. The pulse train is focused down to a spot size of 7 μm radius (FWHM) at

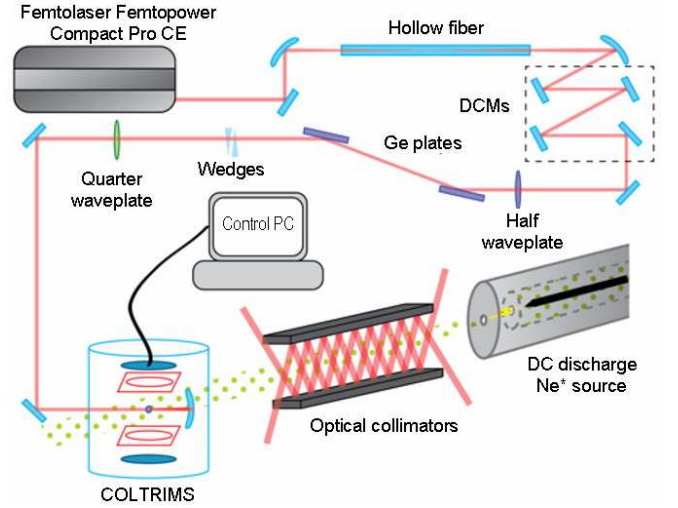


FIG. 1: Schematic representation of the experiment

the interaction region of the commercially available Cold Target Recoil Ion Momentum Spectroscope (COLTRIMS) from Roentdek. This is the electron detection device, where the laser pulse ionises atoms from a target atom beam, then uses position dependent delay-line time of flight detectors to determine the momentum vectors of the ionized electrons. More information on this device can be found in [18]. The electron momentum is measured as a function of the ellipticity of the ionizing beam, which is varied using a quarter waveplate. The Ar beam is provided by a cold gas jet source. Metastable 3P_2 neon atoms are produced by a gas discharge source, which uses a DC discharge across a supersonic gas expansion region to excite approximately 1% of neon atoms in a gas jet into the correct state. The flux of metastable neon atoms is improved by optical collimation techniques that take advantage of the 640 nm closed optical transition to the 3D_3 state. Further details of this gas source can be found in [19, 20].

Experimental and theoretical TEMD results for Ar are shown in Figure 2. A general trend of the calculated TEMD with increase of ellipticity is very similar to that reported previously for the simulations of the hydrogen atom [9]. The cusp-like structure is present for linear polarization and it gradually evolves into a Gaussian as the ellipticity parameter increases.

Figure 3 presents the theoretical and experimental TEMD results for metastable Ne^* . In this target atom, the TEMD evolution with the ellipticity parameter is very weak with the cusp clearly present even for the circularly polarized pulse. To analyze this cusp in more detail, we zoomed in on the narrow range of momenta $p_{\perp} \in (-0.15, 0.15)$ a.u. in the vicinity of $p_{\perp} = 0$. To enhance the cusp, we visualize the function $V(p_{\perp}) = \ln W(p_{\perp})$ in this narrow interval. For the TEMD $W(p_{\perp})$ to have a cusp at $p_{\perp} = 0$, $V(p_{\perp})$ should have an infinite derivative of some order at this point and have an expansion [9] near $p_{\perp} = 0$:

$$V(p_{\perp}) = B + A|p_{\perp}|^{\alpha}. \quad (5)$$

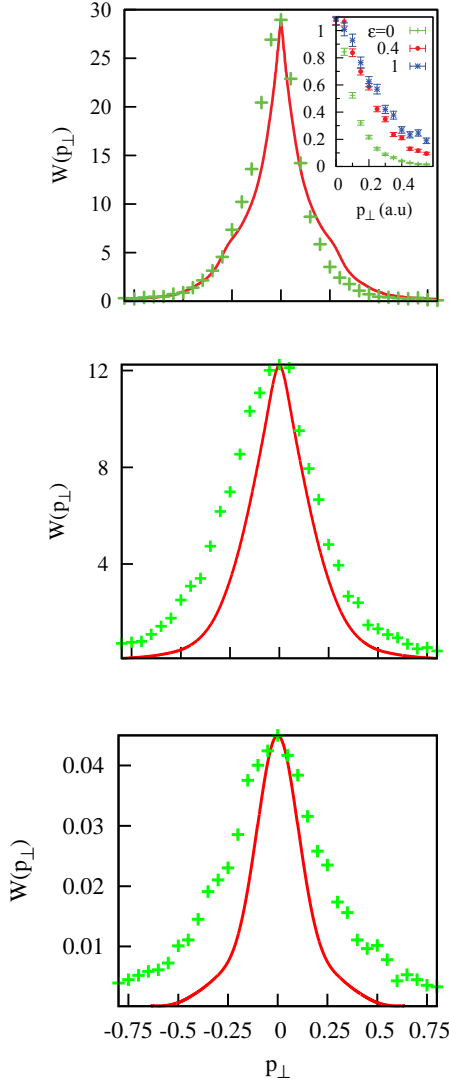


FIG. 2: (Color online) TEMD of Ar (multiplied by 10^3) for ellipticity parameters $\epsilon = 0, 0.47$, and 1 (from top to bottom). TDSE calculation (red) solid curve, experimental data (green) crosses. The peak intensity of the laser pulses were the same as simulation intensities (4.8×10^{14} W/cm 2). Insert shows normalized TEMD with all three experimental measurements overlapped.

This expansion does, in fact, reproduce $V(p_{\perp} \simeq 0)$ very well as is seen in Figure 4 where the calculated $V(p_{\perp})$ and predictions of the fit based on the (5) are displayed.

The same functional form (5) was used to fit both the theoretical and experimental data for the ground state Ar and the metastable Ne* in the whole range of ellipticities by considering the coefficients A, B, α as fitting parameters. The most essential α parameters are shown in Figure 5 for Ar (top) and Ne* (bottom). Shown in the figure are the estimated experimental fitting errors. For the theoretical data, the fitting errors do not exceed a fraction of a percent and are not visible on the scale of the figure. The Ar and Ne* data in Figure 5 show a qualitatively different behavior of the α parameter as

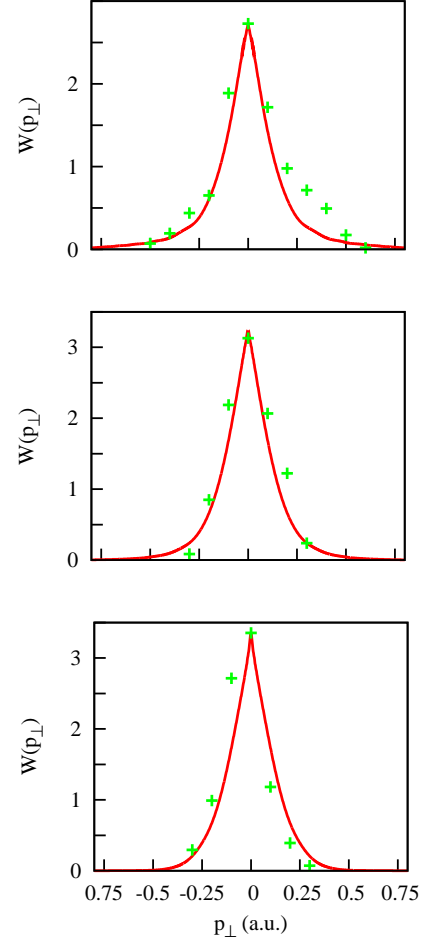


FIG. 3: (Color online) TEMD of metastable Ne* for ellipticity parameters $\epsilon = 0, 0.42$, and 1 (top to bottom). TDSE calculation (red) solid curve, experimental data (green) crosses. The peak intensity of the laser pulses were the same as simulation intensities (2×10^{14} W/cm 2). Fewer data points were taken due to the requirement of longer data collection times. This was required as a result of reduced atomic flux.

a function of the ellipticity. For the Ar atom, the α parameter grows with ϵ reaching the value close to 2 for circular polarization, implying that TEMD becomes close to a Gaussian for the ellipticity parameter values approaching 1. However, for the metastable Ne* atom, the α parameter remains essentially flat, indicating that a cusp-like behavior is present for all ϵ in the range from linear to circular polarization.

While the Ar case shows the behavior qualitatively similar to that found previously for hydrogen [9], the metastable Ne* presents a different trend, with the cusp never disappearing completely. In this case, a simplified description (4) based on the Keldysh theory is never correct even qualitatively. This qualitative difference can be explained by the different ionization regimes for Ar and metastable Ne*. Indeed, the critical field corresponding to the onset of OBI can be found from the equation $E_{\text{obi}} = (I + \Delta I_{\text{AC}})^2/4$, where ΔI_{AC} is the AC Stark shift of the ionization potential. This simple formula for E_{obi}

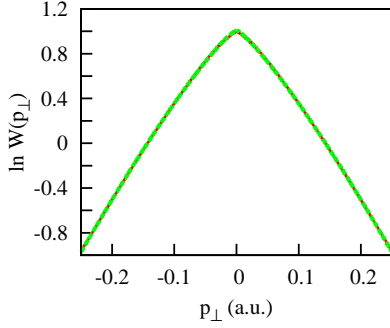


FIG. 4: (Color online) The logarithmic TEMD $V(p_{\perp}) = \ln W(p_{\perp})$ (red solid line) and predictions of the fit based on (5) (green dots) for metastable Ne^* driven by the linearly polarized pulse.

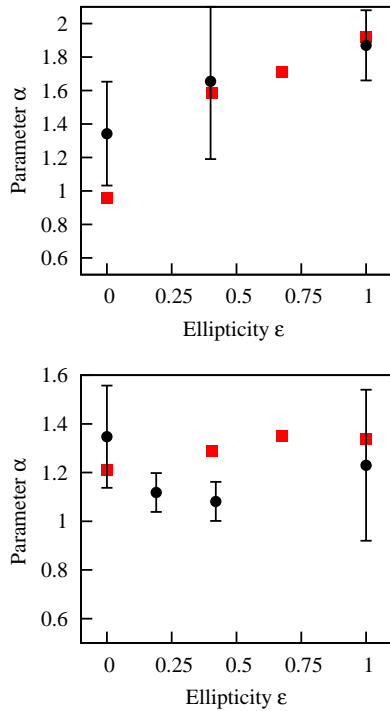


FIG. 5: (Color online) The fitting parameter α in Eq. (5) as a function of the ellipticity parameter ϵ for Ar (top) and Ne^* (bottom). (Black) circles: experimental data, (red) squares: theoretical results.

does not take into account the possibility of the above-barrier reflection [4], but for the weak fields that we presently consider it should provide a good estimate. By approximating the AC Stark shift as $\Delta I_{\text{AC}} \approx E^2/(4\omega^2)$, we obtain for the metastable Ne^* $E_{\text{obi}}^{\text{Ne}^*} \approx 0.0093$ a.u. which is less than the field $E = 0.0756$ a.u. that we employ. An analogous estimate for Ar shows that the intensity of 4.8×10^{14} W/cm² we employ for Ar is well into the tunneling ionization domain.

The TEMD cusp disappearance with increasing ϵ can be explained by the dramatic change of the angular momentum composition of the ionized electron wave function [9]. This angular momentum composition can be conveniently charac-

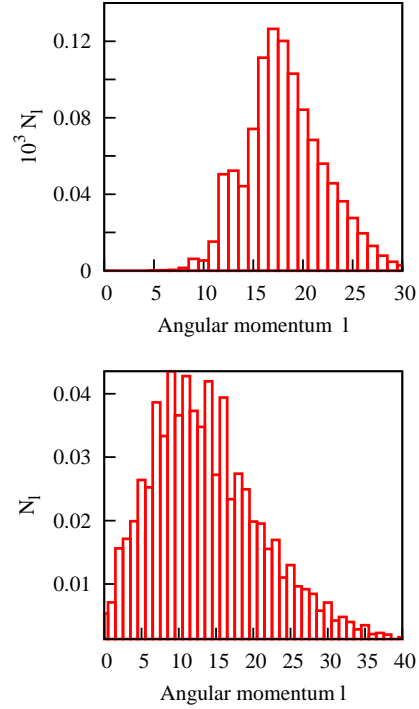


FIG. 6: (Color online) Distribution $|N_l|^2$ for hydrogen for laser field intensities of 10^{14} W/cm² (top) and 10^{15} W/cm² (bottom). Laser field is circularly polarized.

terized by the distribution of the norm N_l of the wave function obtained if only the terms containing spherical harmonic of the rank l are retained in expansion (2). For a tunneling process we can expect this distribution to be shifted towards larger l with increasing pulse ellipticity parameter. Indeed, a tunneling process can be viewed as a non-resonant absorption of a large number of photons. Absorption of a photon from the circularly polarized wave increases the magnetic quantum number by one unit. This leads to a prevalence of high angular momenta in the partial wave expansion (2). High angular momenta create large centrifugal barrier, which suppresses the Coulomb focusing effects that are responsible for the cusp-like behavior. The cusp, therefore, vanishes for polarization close to circular, as in the case of Ar reported here, or hydrogen reported earlier [9]. The situation with the metastable Ne^* is completely different. OBI dominates in this case, and since OBI is essentially a distortion of the atomic potential to the degree, that there is effectively a zero barrier to the continuum, the atom does not have to absorb many photons to become ionized. We may expect, therefore the distribution N_l to be peaked at the values of the angular momenta lower than in the case of tunneling. That this is indeed the case can be seen in Figure 6, where the distributions N_l are shown for hydrogen for the circularly polarized pulse with the field intensities of 10^{14} W/cm² (tunneling) and 10^{15} W/cm² (the OBI regime). Smaller angular momenta enhance the area near the origin where the Coulomb focusing effect is strongest. Larger angular momentum components are repelled from the origin due

to the centrifugal barrier. Hence in the former case the cusp is always present whereas in the latter case it gradually vanishes. This corresponds to a classical trajectory starting from the origin whereas a tunneling trajectory starts at the point of exit from the tunnel.

To summarize, we described an effect of bending the Coulomb barrier of the atom on the transverse electron momentum distribution (TEMd) in strong field ionization in the tunneling regime. This fundamental effect, which should be present in any atomic or molecular target, is measured experimentally and modeled theoretically in two vastly different species: the ground state Ar and metastable Ne*. The effect

is substantial, it has never been described or observed before and has to be taken into account when using TEMd data to interrogate electronic structure of the target. The fact that the TEMd behaves in a markedly different way for the tunneling and OBI regimes enables a clear distinction between these two regimes in the experiment.

We acknowledge support of the Australian Research Council in the form of the Discovery Project DP120101805 and DP110101894. Resources of the National Computational Infrastructure (NCI) Facility were employed. JEC was supported by an Australian Postgraduate Award.

-
- [1] F. Krausz and M. Ivanov, *Rev. Mod. Phys.* **81**, 163 (2009).
 - [2] L. V. Keldysh, *Sov. Phys. -JETP* **20**, 1307 (1965).
 - [3] S. Augst, D. D. Meyerhofer, D. Strickland, and S. L. Chin, *J. Opt. Soc. Am. B* **8**, 858 (1991), URL <http://www.opticsinfobase.org/josab/abstract.cfm?URI=jds3b-4-858>.
 - [4] N. B. Delone and V. P. Krainov, *Physics-Uspekhi* **41**, 469 (1998).
 - [5] F. H. M. Faisal, *J. Phys. B* **6**, L89 (1973).
 - [6] H. R. Reiss, *Phys. Rev. A* **22**, 1786 (1980).
 - [7] A. Rudenko, K. Zrost, T. Ergler, A. B. Voitkiv, B. Najjari, V. L. B. de Jesus, B. Feuerstein, C. D. Schröter, R. Moshhammer, and J. Ullrich, *J. Phys. B* **38**, L191 (2005), URL <http://stacks.iop.org/0953-4075/38/i=11/a=L01>.
 - [8] L. Arissian, C. Smeenk, F. Turner, C. Trallero, A. V. Sokolov, D. M. Villeneuve, A. Staudte, and P. B. Corkum, *Phys. Rev. Lett.* **105**, 133002 (2010).
 - [9] I. A. Ivanov, *Phys. Rev. A* **90**, 013418 (2014).
 - [10] A. S. Kheifets and I. A. Ivanov, *Phys. Rev. A* **90**, 033404 (2014).
 - [11] A. N. Pfeiffer, C. Cirelli, A. S. Landsman, M. Smolarski, D. Dimitrovski, L. B. Madsen, and U. Keller, *Phys. Rev. Lett.* **109**, 083002 (2012), URL <http://link.aps.org/doi/10.1103/PhysRevLett.109.083002>.
 - [12] I. Dreissigacker and M. Lein, *Chem. Phys.* **414**, 69 (2013), URL <http://www.sciencedirect.com/science/article/pii/S0301010412003416>.
 - [13] A. S. Kheifets, F. J. Gálvez, and E. Buendia, *At. Data Nucl. Data Tables* **88**, 163 (2004), URL <http://www.sciencedirect.com/science/article/pii/S0092640X04000040>.
 - [14] I. A. Ivanov, *Phys. Rev. A* **82**, 033404 (2010).
 - [15] I. A. Ivanov, *Phys. Rev. A* **83**, 023421 (2011).
 - [16] M. Nurhuda and F. H. M. Faisal, *Phys. Rev. A* **60**, 3125 (1999).
 - [17] V. S. Popov, *Physics-Uspekhi* **47**, 855 (2004).
 - [18] H. Xu, J.-P. Maclean, D. Laban, W. Wallace, D. Kielpinski, R. Sang, , and I. Litvinyuk, *New J. Phys.* **15**, 023034 (2013), URL <http://iopscience.iop.org/1367-2630/15/2/023034/article>.
 - [19] M. Baker, A. Palmer, and R. Sang, *Meas. Sci. Technol.* **14**, N5 (2003), URL <http://iopscience.iop.org/0957-0233/14/4/401>.
 - [20] A. Palmer, M. Baker, and R. Sang, *Rev. Sci Instrum.* **75**, 5056 (2004).